Volume 1 | Number 1 | Jan 2013 | Pages 1–100

PCCP

Physical Chemistry Chemical Physics
www.rsc.org/pccp

ROYAL SOCIETY OF CHEMISTRY

This is an *Accepted Manuscript*, which has been through the Royal Society of Chemistry peer review process and has been accepted for publication.

*Accepted Manuscripts* are published online shortly after acceptance, before technical editing, formatting and proof reading. Using this free service, authors can make their results available to the community, in citable form, before we publish the edited article. We will replace this *Accepted Manuscript* with the edited and formatted *Advance Article* as soon as it is available.

You can find more information about *Accepted Manuscripts* in the **Information for Authors**.

Please note that technical editing may introduce minor changes to the text and/or graphics, which may alter content. The journal's standard **Terms & Conditions** and the **Ethical guidelines** still apply. In no event shall the Royal Society of Chemistry be held responsible for any errors or omissions in this *Accepted Manuscript* or any consequences arising from the use of any information it contains.

# Journal Name

## ARTICLE

# Tuning the Thermal Conductivity of Solar Cell Polymers through Side Chain Engineering

Zhi Guo[a], Doyun Lee[b], Yi Liu[c], Fangyuan Sun[a,e], Anna Sliwinski[b], Haifeng Gao[b], Peter C. Burns[c], Libai Huang[d], and Tengfei Luo[a]*

Thermal transport is critical to the performance and reliability of polymer-based energy devices, ranging from solar cells to thermoelectrics. This work shows that the thermal conductivity of low band gap conjugated polymers, poly(4,8-bis-alkyloxybenzo[1,2-b:4,5-b']dithiophene-2,6-diyl-alt-(alkylthieno[3,4-b]thiophene-2-carboxylate)-2,6-diyl) (PBDTTT), for photovoltaic applications can be actively tuned through side chain engineering. Compared to the original polymer modified with short branched side chains, the engineered polymer using all linear and long side chains shows a 160% increase in thermal conductivity. The polymer thermal conductivity exhibits a good correlation with the side chain lengths as well as the polymer crystallinity characterized using small-angle X-ray scattering (SAXS) experiments. Molecular dynamics simulations and atomic force microscopy are used to further probe the molecular level local order of different polymers. It is found that the linear side chain modified polymer can facilitate the formation of more ordered structures, as compared to the branched side chain modified ones. The effective medium theory modelling also reveals that the long linear side chain enables larger heat carrier propagation length and the crystalline phase in the bulk polymer enlarges the overall thermal conductivity. It is concluded that both the length of the side chains and the induced polymer crystallization are important for thermal transport. These results offer important guidance for actively tuning thermal conductivity of conjugated polymers through molecular level design.

## Introduction

Low band gap conjugated polymers are emerging as an important class of material that exhibit great potential for low-cost, lightweight, and flexible energy and electronic devices.[1-3] Recent progress in synthesizing low band gap conjugated polymers has led to a variety of promising candidates.[4-8] In particular, polymer solar cells (PSCs) based on poly(4,8-bis-alkyloxybenzo[1,2-b:4,5-b']dithiophene-2,6-diyl-alt-(alkylthieno[3,4-b]thiophene-2-carboxylate)-2,6-diyl) (PBDTTT) conjugated copolymer reach a record-high power conversion efficiency of 7-10%,[9, 10] which is significantly higher than the Poly(3-hexylthiophene-2,5-diyl) (P3HT) based counterparts whose highest efficiency is 3-5%.[11, 12] Efficiency and stability are two major issues in advancing PSC technologies. While charge transport has been extensively studied in PSC materials to improve their efficiency, thermal transport is largely ignored. The thermal transport in PSCs is an important factor that influences their performance and lifetime because extended operation at elevated temperature accelerates degradation of the organic molecules, as well as impairing their efficiency.[13, 14] Sunlight and weather can lead to temperature variation in PSCs, as can the heat generated in futile charge recombination processes. Considering the low efficiency of PSCs, the majority of the solar energy received is converted into heat. However, the low thermal conductivity of amorphous polymers[15] hampers the heat transfer from the cell to the environment, resulting in an increase in cell temperature. It is thus critical to account for the thermal transport properties of the conjugated polymers when designing new materials for PSC applications.

Moreover, an increasing number of conjugated polymers are being explored for thermoelectric applications.[16-20] For thermoelectric materials, low thermal conductivity is desirable, which can in turn increase the figure of merit, ZT.[21] However, methods that can further reduce the already low thermal conductivity of amorphous polymers are rare.

Thus far, only limited amount of work has been directed towards understanding the thermal properties of organic photovoltaic materials. Recent work on P3HT has shown very low thermal conductivity, yet the thermal conductivity measured from films of various thicknesses reported by different groups using various techniques are very consistent,[22, 23] indicating that the thermal transport in these materials is at the diffusive limit. The thermal conductivity of another organic semiconductor, copper phthalocyanine (CuPc), has been reported to be around 0.39 W m$^{-1}$ K$^{-1}$.[24] The thermal conductivities of widely used conductive polymers poly(3,4-ethylenedioxythiophene) (PEDOT) and poly(3,4-ethylenedioxythiophene): poly(styrenesulfonate) (PEDOT:PSS) thin films were measured using the 3ω technique and time domain thermoreflectance (TDTR), respectively.[22, 25] Duda et al. found an ultra-low thermal conductivity for [6,6]-phenyl-C61-butyric acid methyl ester (PCBM) (~0.03 W m$^{-1}$ K$^{-1}$)[26] using the TDTR technique and a simple linear dependence of thermal conductivity on the mixing ratio of P3HT:PCBM bulk heterojunction was observed.[22]

The PBDTTT family of polymers are promising alternatives to P3HT given their proven higher efficiency when they are blended with PCBM.[9, 10] Their thermal transport properties, however, are unknown. In amorphous polymers, the thermal conductivity is related to the heat carrier propogation length,[27] which is closely related to the local order of atom arrangements – a factor influenced by the molecular structure. It has also been shown that the thermal conductivity is a strong function of morphology.[21, 28-31] Tuning the crystallinity of polymers can change the thermal conductivity by orders of magnitude.[28-30] An advantage of the PBDTTT family of polymers is the multiple modification sites that are available for tuning the molecular structure which does not only influence the local order in the amorphous phase but also influence polymer crystallinity. Side chain tuning has been utilized to achieve better performance in PSCs[32-35].

In this work, we show that proper engineering of the side chains on the PBDTTT polymers can actively tune their thermal conductivities. The thermal conductivity was measured using TDTR, and the crystallinity was characterized using small-angle X-ray scattering (SAXS). The local order of the polymer is also probed using atomic force microscopy (AFM) and molecular dynamics (MD) simulations. By using proper side chains, the thermal conductivity of the polymer was enhanced by as much as 160%. Such an enhancemant is then anlayzed using effective medium theory and the mechanism is understood.

## 1. Sample preparation

The molecular structure of PBDTTT polymer is shown in Figure 1. The PBDTTT polymer backbones are modified with three substituted solublizing groups. The alkyl side chain groups on R1 and R2 positions include two types: 1) ethylhexyl group (branched structure, $C_6+C_2$, denoted as E) that provides solubility and processibility for polymers and 2) dodecyl group (linear structure, $C_{12}$, denoted as D) that can enable high crystillinity. Their combination results in four different substituted polymers on PBDTTT backbone: PBDTTT-EE, PBDTTT-ED, PBDTTT-DE, and PBDTTT-DD, in which the first letter indicates the two identical substituted groups on BDT unit and the second letter indicates the substitutied groups on TT unit. Detailed polymer synthesis can be found in the Supporting Material. The polymers were first dissolved in chlorobenzene at a concentration of 20 mg/mL. The solutions

were then used for film preparation in two ways. One approach was spin casting the solution on glass substrates (VWR Inc.) or silicon wafers (Graphene supermarket, Reading, MA, USA) at 1500 RPM for 30 seconds to form films. The film thickness ranged from 41 nm to 64 nm as determined by profilometry (KLA-Tencor P6). To obtain thick films that can be used in SAXS experiments, as well as to test if there is any film thickness dependence in TDTR experiments, the drop casting method was also used to produce films thicker than 1 μm. A 100 nm thick Al film (nominal thickness) was then deposited using electron beam evaporation on top of the polymer film for TDTR measurements. Samples were placed in a vacuum chamber throughout the experiment to prevent possible oxygen/moisture-induced degradation during measurements.
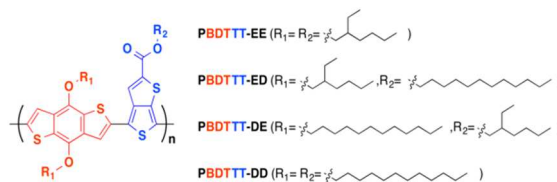


**Figure 1**. Molecular structure of PBDTTT polymers. The red part is the BDT unit connected with two symmetric R1 substitution sites, and the TT unit connected with R2 substitution site is shown in blue. Four polymers composed of different alkyl side chain substituion combinations.

## 2. Time-domain thermoreflectance (TDTR) measurements

The TDTR measurements were performed using a 800 nm pulsed laser (100 fs pulse duration, 80 MHz repetition rate) output from a Ti-sapphire oscillator (Spectra Physics) as the probe, and a pump beam centered at 400 nm after frequency doubling with a Bismuth Borate (BIBO) non-linear crystal for heating. The probe beam was delayed with respect to the pump beam by double-passing a mechnical delay stage, which yielded up to 6 ns delay time. The pump and probe beams were directed colinearly towards the Al film surface and focused using an objective lens (Edmond Optics, 10x), yielding an $1/e^2$ radii of 50 um and 9 um, respectively. A CCD camera was used as a microscope to ensure that a good sample surface was studied, which is especially important for drop casting film, which can contain micro air bubbles on the surface, which needs to be avoided in TDTR experiments. The pump light intensity was modulated by an electro-optical modulator (350-160, Conoptics Inc.) at 5 MHz. The reflected probe light from the sample surface was directed to a photodiode detector (PDA36A, Thorlabs Inc.) with an amplification gain of 3x. The amplitude as well as the phase signals were demodulated by a lock-in amplifier (SRS 844, Stanford Research System). The total laser power on the sample was kept under 30 mW, and the estimated steady state temperature rise was about 10~25 K.[36] For each polymer film measurement, the thermoreflectance decay curve was obtained by averaging over 40 scans. The thermoreflectance decay curve, which is propotional to temperature decay, was fitted to a heat transfer model with pulse accumulation effects to extract the thermal conductivity of the polymers. More details of these measurements are well documented in other references [36, 37].

Since the heat transfer model is sensitive to the thickness of the Al film, we determined the thickness from the acoustic echo of the thermoreflectance signal. We calculated the thickness of the aluminum film using $d = \frac{1}{2}vt_{echo}$, where v=6260 m s$^{-1}$ is the velocity of sound in aluminum. Since the echo period was about 31 ps (see inset in Figure 2), the film thickness is estimated to be 97 nm. This value was used for data fitting.

The amplitude decay from TDTR measurements for the four different polymer films is presented in Figure 2. We used a heat transfer model to fit the amplitude data and extract the thermal conductivity.[36, 37] In the heat transfer model, the heat capacity must be known for all materials in order to calculate the thermal conductivity. The heat capacity of Al is standard, and a value of $2.52 \times 10^6$ J m$^{-3}$ K$^{-1}$ was used.[38] The heat capacity of the PBDTTT polymer was determined from the heat flow curve measured by differential scanning calorimetry (DSC), assuming the density of the PBDTTT polymer to be 1.0 g cm$^{-3}$, a value used for a similar polymer PCPDTBT.[39] We do not expect this assumption to influence the validity of the conclusion of this work since the densities of this group of polymers should not vary much. The measured heat capacities for the PBDTTT polymers are around $2.8 \times 10^6$ J m$^{-3}$ K$^{-1}$ and the variation among the polymers is within 5% (for measured DSC curves and heat capacity calculations, see the Supporting Material).
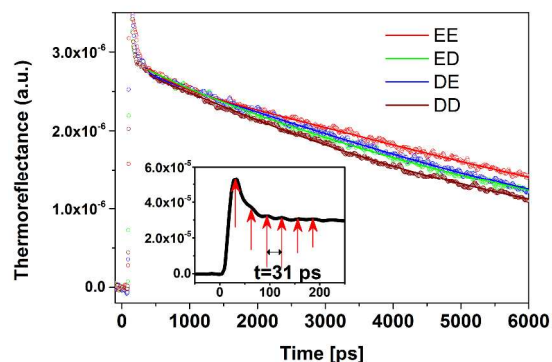


**Figure 2.** Thermal reflectance decay in four side chain-substituted PBDTTT polymers, all measured with a 5 MHz modulation frequency. Inset: Acoustic echoes with equal spacing indicated by red arrows. The time interval between consecutive echoes is 31 ps. Best fits from the heat transfer model are represented by solid lines. The thermoreflectance values are normalized and have arbitrary units.

The thermal conductivity and interfacial thermal conductance obtained from fitting to the heat transfer model for all four polymers are summaried in Table 1. The thermal conductivities measured in the spin cast (thin) films and the drop cast (thick) films are in good agreement. The discrepancies between them are within the uncertainty obtained from sensitivity analyses, indicating that the thermal conductivity has little dependency on film thickness. This finding is in agreement with previous work on P3HT films.[22, 23] It is worth noting that interfacial thermal conductance values are all small and fall within the range of the thermal conductance of weak van der Waals interfaces (10-50 W m$^{-1}$ K$^{-1}$).[21] This finding is consistent with the fact that one prerequisite of allowing the determination of film thickness via acoustic echo is a weak interface.[40] In general, due to the low thermal conductivity of polymers that

dominates the thermal resistance, the heat transfer model used in fitting is not sensitive to the interfacial thermal conductance. The most significant finding from Table 1 is the dramatic increase in the thermal conductivity as the side chains of the polymers change from short and branched functional groups (EE) to long and linear groups (DD). Such a trend is believed to be closely related to the characteristics of the side-chains and the induced crystallization of the bulk polymers as studied in the following sections.

**Table 1.** The thermal conductivities of four polymer films prepared from spin casting and the corresponding interfacial thermal conductance determined by fitting the thermoreflectance data. In the thermal conductivity column, values in the brackets are obtained from similar measurements on the thick, drop casted films. Uncertainties are obtained from sensitivity analyses similar to that documented in reference.[35]

| Polymer | Thermal conductivity (W m$^{-1}$ K$^{-1}$) | Interfacial thermal conductance (W m$^{-2}$ K$^{-1}$) |
|---------|--------------------------------------------|-------------------------------------------------------|
| EE | $0.10 \pm 0.02$ ($0.12 \pm 0.02$) | 13 |
| ED | $0.20 \pm 0.03$ ($0.21 \pm 0.03$) | 26 |
| DE | $0.19 \pm 0.03$ ($0.22 \pm 0.03$) | 44 |
| DD | $0.26 \pm 0.04$ ($0.29 \pm 0.04$) | 45 |

## 3. Crystallinity in different polymers

To study the morphologies of different polymers, we performed SAXS measurements (Bruker NANOSTAR, Cu source, λ=0.154184 nm) that are able to characterize the periodic structures and their ordering in materials. The data from SAXS can be analyzed to study the degree of crystallinity and crystalline domain size of materials. More details on the SAXS measurements can be found in the Supporting Material. Figure 3 shows the scattering patterns of all four polymer films
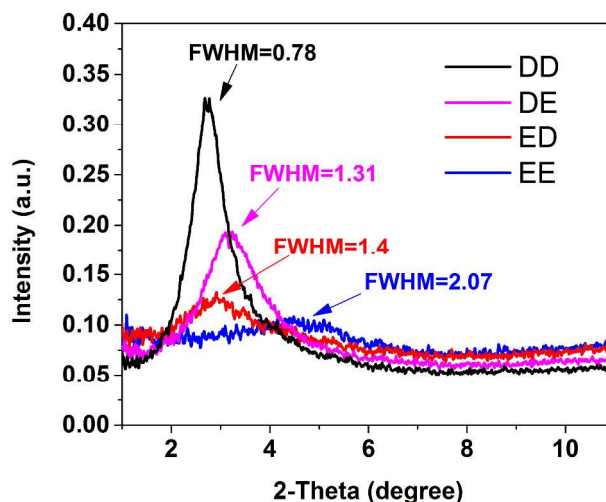


**Figure 3.** Angular scattering from SAXS experiments of the four polymers. The scattering intensities of all the polymers are after substrate background subtraction and has been normalized by their sample thicknesses using glassy

carbon calibration within the surveyed angle range. The full width half maximum (FWHM) of the scattering peak has been calculated and labeled.

The size of the crystallite can be characterized by analyzing the lineshape widths of diffraction peaks using the Scherrer's equation[41]: narrower peaks indicate larger crystallites. The estimated crystallite sizes range from 4 to 10 nm (see Table 2). The crystallinity of the polymers can also be estimated by calculating the percentage of crystalline polymer scattering peak intensity with respect to the total scattering intensity, which is also shown in Table 2.

**Table 2.** Crytallite size, crystallinity, and d-spacing calculated from SAXS/GISAXS data for the four different polymers. Values in the bracket are obtained from GISAXS measurements in Figure 5. The last column shows the lengths of the two longest side chains length added together in corresponding molecules.

| Polymer | Crystallite size (nm) | Crystallinity | d-spacing (nm) | Two side chain length (nm) |
|---------|-----------------------|---------------|----------------|----------------------------|
| EE | 4 (4.0) | 6.6% | 1.7 (1.9) | 1.68 |
| ED | 6 (4.4) | 8.8% | 3.1 (2.2) | 3.1 |
| DE | 6 (6.5) | 20% | 2.8 (2.7) | 3.1 |
| DD | 10 (8.5) | 30% | 3.3 (3.1) | 3.1 |

# 4. Molecular-level structure characterization

To further explore the molecular-level structural characteristics of the four polymers, we extracted the d-spacing information from the 2-theta angles of the diffraction peak in the SAXS data (Figure 3). The corresponding d-spacing information found in different polymer films is summarized in Table 2. We observe that the d-spacing are close to the sum of the length of the two longest side chains of the corresponding polymer molecules. Therefore, the molecular packing in the nanocrystallites is postulated to be a lamellar structure between the polymer chains separated by their longest side chains (a schematic view of PBDTTT-EE is shown in Figure 4). The lamellar packing order of this type polymer backbone has previous been reported in Gazing incident wide angle X-ray scattering (GIWAXS) experiments.[13, 33] In these reports, it is suggested that there is an orientation preference in the packing of this type of copolymer. There are more backbone lamellae stacked in parallel to the substrate surface, while the side-by-side inter-polymer packing emerges as an in-plane order. The Gazing incident small angle X-ray scattering (GISAXS) experiments have been performed on the polymer films on silicon substrates to investigate structural order along different directions in thin films (for details, see Supporting Material). In Figure 5, the GISAXS pattern of four polymers all reveal a preferred in-plane order with d-spacing values similar to those found in SAXS experiments, which implies the existence of the lamellar structure and the π-π stacking order. To further verify the existence of such an order in our work, AFM studies have been performed (for details, see Supporting Material). It is shown in figure S3 (in Supporting Material) that ordered crystalline grains are found in PBDTTT-DD polymer film surface. For those grains that have few

lamellae layer differences, the height differences consistently falls in between 3.7 and 4 Å, which is the characterisitc π-π stacking distance and is in good agreement that found in a PTB polymer modified with linear side chains of similar length (PTB1[33], 3.65 Å). By dividing the crystallite size by the d-spacing, the average number of lamellar layers in a nanocrystallite mentioned above varies from 2 (in EE) to 3 (in DD).
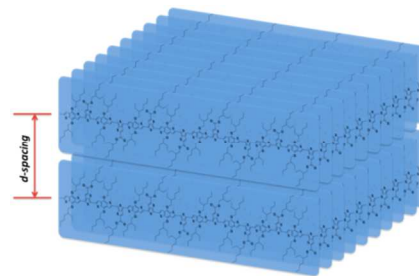


**Figure 4.** Schematic view of the lamellar structure of PBDTTT-EE polymer. The d-spacing of the periodic structure is determined by the spacing of two backbones. In this case, it is roughly the sum of two side chain lengths.
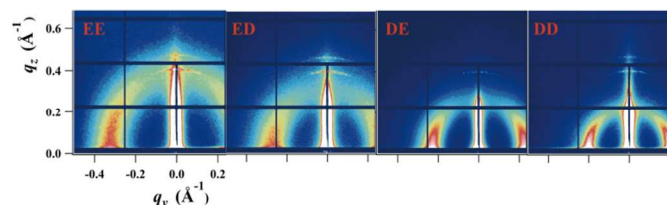


**Figure 5.** GISAXS patterns from four polymer films (λ=0.8856 Å), from left to right: EE, ED, DE and DD. The horizontal scales for all four panels are the same. To obtain the d-spacing information, the in-plane line cut is chosen at $q_z=0.03$ Å$^{-1}$. The scattering peaks were fitted with Gaussian functions. The d-spacing and lateral crystallite sizes were summarized in the Table 2.

To gain insight into the local order in the polymers, we performed MD simulations to study the self-assembly of the polymer molecules. The EE and DD polymers were selected as the two extremes to demonstrate the differences in local orders. In these simulations, hexamers (six repeating units) were used to model the polymer chains and 35 hexamers were used to simulate the self-assembly. The OPLS-2005 (Optimized Potentials for Liquid Simulations) force field was used to model the molecular interaction in the conjugated polymers.[42] This force field has been successfully applied to predict a variety of P3HT configurations and can yield results consistent with experimental findings.[43-45] Recent benchmarks on a series of low band gap conjugated polymer, including PBDTTT, also show that this force field can describe the torsional potential surface behavior quantitatively with accuracy comparable to high-level quantum chemistry calculations.[45, 46]

The simulation was performed in NVT (constant number of atoms, constant volume and constant temperature) ensemble at 400 K with periodic boundary conditions applied in all three spatial directions. The Desmond code (D.E. Shaw Research Inc.)[47] was used. The system temperature was set close to the experiment annealing temperature, which allows the system to sample a broader potential surface and thus have a greater chance of escaping from local minima structures. The equation of motion was integrated with a 2 fs step size with all bonds connected to hydrogen atoms constrained using the M-SHAKE

sheme[48]. The trajectories were recorded for 60 ns at a 10 ps interval. Figure 6 shows the initial random configuration of DD and EE polymers together with their self-assembled structures after 60 ns. Although the simulation time is far from sufficient for capturing a complete phase transition of such a glassy system, DD molecules are able to form a more ordered and compact structure compared to EE molecules on the same time scale.
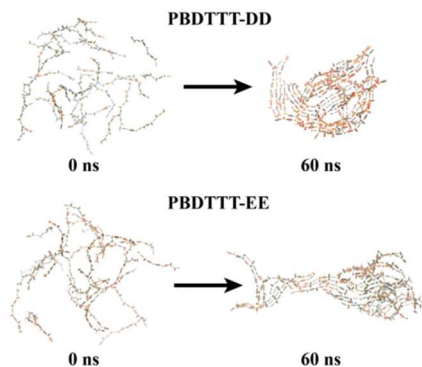


**PBDTTT-DD**

0 ns          60 ns

**PBDTTT-EE**

0 ns          60 ns

**Figure 6.** The initial (0 ns) and final (60 ns) structures of PBDTTT-DD and PBDTTT-EE from MD simulations. For clarity, only the backbones are shown.

A more quantitative approach to analyze the structural change is to use the radial distribution function. In order to show the evolving trend of these two polymers during self-assembly, we define the difference pairwise radial distribution function $\Delta\Re(r)$, which is expressed as a relative change of the pairwise radial distribution function of the final structure compared to that of the initial structure. First, the pairwise radial distribution function of two atom groups is defined as:

$$R(r) \ = \ g(\mathbf{r_1}, \mathbf{r_2}), \quad (1)$$

$\mathbf{r_1}$ and $\mathbf{r_2}$ are the position vectors of two atoms, and $r = \left|\mathbf{r_1} - \mathbf{r_2}\right|$. Then the difference pairwise radial distribution function $\Delta\Re(r)$ is calculated as:

$$\Delta\Re(r) \ = \ R_{60\,ns}(r) - R_{0\,ns}(r) \qquad (2)$$

Here, we select all the sulfur atoms in the system to represent both the reference ($\mathbf{r_1}$) as well as the objective ($\mathbf{r_2}$) atom groups. In Figure 7, we see a population increase over a broad range of radial distances (0-7.5 nm), and a minor decrease of population beyond that (>7.5 nm) in both DD and EE polymers, suggesting an aggregating trend. Within 1.2 nm, the population increase appears more like discrete peaks. A close examination shows that these peaks correspond to certain intra-chain geometry constraints enforced by the lamellar π-π stacking of the backbones, which is due to the planar backbone that contains fused-benzene rings in these type of polymers. Compared to EE, the DD polymer shows a higher intra-chain order, implying better π-π planar packing in DD. The average π-π stacking distance obtained from the MD simulation is around 4.1Å, (averaged over interlayer sulfide atom mesaured in the

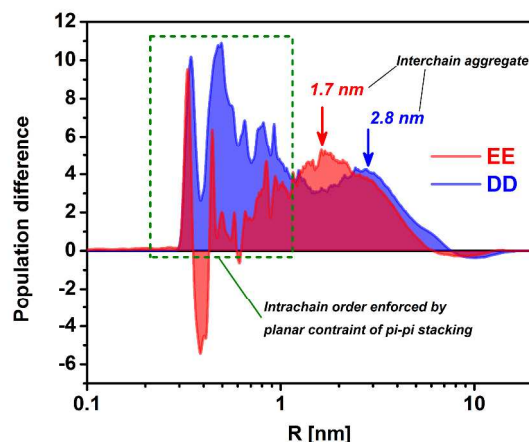structures), which is in good agreement with our AFM measurements.



**Figure 7.** Difference radial distribution function $\Delta\Re(r)$ of sulfur atoms in the PBDTTT-DD(blue) and PBDTTT-EE(red) polymer aggregates. The intrachain orders enhanced due to self-assembly induced π-π stacking are emphasized in a green dash box.

It has been shown that the intra-chain order enhanced by interchain packing can significantly enhance the thermal conductivity in crystalline polymers.[30] The ordered backbone will present less phonon scattering inside the chain due to less structural disorder along the backbone. In addition, we find broad and smooth peaks located at 1.7 nm and 2.8 nm for EE and DD polymers, respectively. These correspond to d-spacings extracted from the SAXS data (Table 2), supporting our hypothesis of the side-by-side packing of the molecules (see Figure 4). The value (2.8 nm) for DD is slightly below the d-spacing resolved in the SAXS experiment. This is probably because of the difference in temperature between the MD simulation (400 K) and experiment (300 K), as the longer linear alkane side chain can adopt a more coiled configuration at higher temperatures.[30, 31] However, due to the low mobilities of the molecules at lower temperature, we are not able to perform simulations on the self-assembly at 300 K within a reasonable simulation time.

Although our MD simulation could not predict the long range order in the highly crystallized structures, it does indicate the better capability of forming more ordered structures of DD. More importantly, the simulation suggests that even the amorphous phase can have different local orders in different polymers, and a key characteristic length, the d-spacing, is captured in the local order. Such a characteristic length can be an important factor that is responsible for the different thermal conductivities in the four polymers, since the diffusion lengths of heat carriers in amorphous materials are influenced by the characteristic lengths of local orders.[21]

## 5. Mechanism of Side Chain-Influenced Thermal conductivity

To understand the mechanism of the thermal conductivity change in different polymers, we relate the structural information obtained from expertiments and MD simulations to the measured thermal conductivity. In a polymer with low crystallinity, such as PBDTTT-EE, molecular structures are more disordered. In disordered structures, the heat transfer is dominated by diffusive transport through extended modes – known as diffuson.[49] The diffusion length of these heat carriers is strongly related to the local atomistic order of the amorphous phase. In a polymer with high crystallinity, such as PBDTTT-DD, heat carriers can be coherent lattice waves (phonons) within the crystalline domain that can travel long distances and transport heat efficiently. In highly ordered single crystal polymers, the efficient phonon transport can enable thermal conductivity on the order of 10 W m$^{-1}$ K$^{-1}$.[28, 50] However, in the bulk polymers studied in this work, the materials will not be single crystals, but instead will contain domains of crystallized regions embedded in an amorphous matrix, forming a compoiste. Such domains, as measured from SAXS (Table 2), has sizes ranging from 4-10 nm. At such small scales, significant size effect exist for thermal transport in the crystalline domain due to the boundary phonon scattering that limits the phonon mean free path. For example, the thermal conductivity of a single crystal of GaAs will decrease by one order of magnitude if the size changes from 10 to 3 nm.[51] The crystalline polymer domains are embedded in the amorphous polymer matrix of low thermal conductivity, and there is thermal boundary resistance between the two different domains. The size of the crystallites and the crystallinity combine to influence their total interface area and thus the overal thermal transpor efficient across the interfaces between the crytalline domain and the amorphous matrix. The measured thermal conductivity are expected to be influenced by these factors, including amorphous domain thermal conductivity, crystallite thermal conductivity and interfacial thermal resistance. To analysis these factors, we study the measured thermal conductivity in such a composite-like material using the effective media theory.[52]
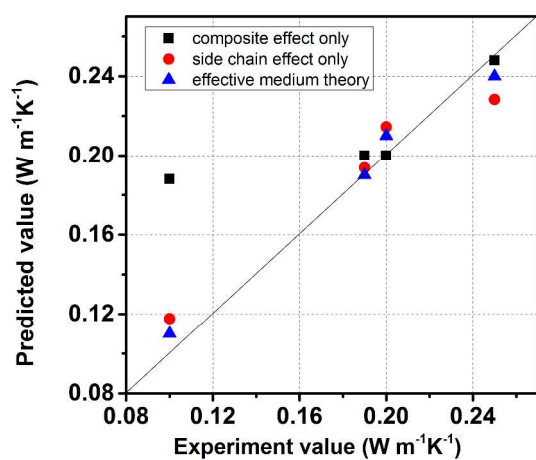


**Figure 8.** The correlation between effective thermal conductivity of different polymers predicted by three models (amorphous/crystalline phase composite effect, side chain effect, and effective medium theory) and those measured by TDTR.

The effective medium theory we use to describe the effective thermal conductivity is a modified formulation for describing nanocomposites, where the inclusion size is smaller than the phonon mean free path (MFP)[53] (see Supporting Material for modeling details). The crystallinity (volumetric concentration of the crystalline domain) and the crystallite size obtained from SAXS measurements are used as inputs for the effective medium thoery to predict the effective thermal conducitivty of the four polymers (for details, see Supporting Material). We have used three models with different assumptions to investigate the relative importance of different factors.

In the first model, we assume that the amrophous phases of all four polymers have the same thermal conductivity, and only the crystallite size effect and interfacial thermal resistance are taken into account. This model, which only considers the composite effect, can reproduce the thermal conductivity trend in PBDTTT-ED, DE and DD (black squares in Figure 8). However, it fails to reproduce the much lower thermal conductivity of PBDTTT-EE.

We notice that only the EE polymer has a much lower d-spacing – a characteristic length that is inherent not only in the crystallites but also in the local order of the amorphous matrix as predicted from the MD simulations. The heat carrier propogation length in the amorphous structure is closely related to such characteristic lengths. As a result, in the second model, we add another fold of complication to consider the varying thermal conductivity in the amorphous phase as a function of side chain length. As shown in Figure 8 (blue triangle), the thermal conductivity is well reproduced by this model.

We have also studied another case in which only the side chain length is considered as the factor influencing the thermal conductivity. It is found that this model can also largely reproduce the experimental data (red dots in Figure 8). However, the quality is not as good as the second model especially for the DD case. We thus conclude that the thermal conductivity difference between EE and other polymers is largely due to the side chain length, while for ED, DE and DD polymers where the side chain lengths are similar, the level of crystallinity and crystallite size are also important factors that influence thermal conductivity.

It is understood that the ultimate goal of engineering the side chain of conjugate polymers is to improve the overall device performance. Besides the thermal transport property improvements that are achieved by engineering the side chains in this work, it is also very important to understand the impacts of this approach on other aspects of solar cell performance, especially the charge transport aspects. Fortunately, there are many reports showing that putting more linear side chains also improve charge transport properties of solar cell performance. For example, higher crystallinity caused by good side chain packing enables a better hole mobility;[54, 55] better pi-pi stacking induced by linear side chain substitution in PTB polymers provides a higher filling factor;[14, 32] and the formation of lamellae structures in crystalline polymers can be used to tune the bandgap.[1, 56, 57]

## Conclusions

In this work we have shown that the thermal conductivity of PBDTTT polymers can be tuned by properly engineering the side chains at different modification sites. The polymer with linear side chains (PBDTTT-DD) exhibits a thermal conductivity that is 160% higher than that of the PBDTTT-EE,

which has shorter and bulkier branched side chains. Strong correlations between the thermal conductivity measured by TDTR experiments and the values predicted by effective medium theory comprising the contributions from intermolecular spacing (d-spacing), crystallinity and crystallite size suggest that these three factors are important to the thermal transport in the PBDTTT polymers. As a result, our work provides a rational and useful guidance on the design of conjugated polymers to achieve desirable thermal transport properties, which is important for their applications in PSCs, thermoelectrics and other fields.

## Acknowledgements

## Notes and references

[a] Department of Aerospace and Mechanical Engineering, University of Notre Dame, Notre Dame, Indiana, 46556, USA.

[b] Department of Chemistry and Biochemistry, University of Notre Dame, Notre Dame, Indiana, 46556, USA.

[c] Department of Civil and Environmental Engineering and Earth Sciences, and Department of Chemistry and Biochemistry, University of Notre Dame, Notre Dame, Indiana, 46556, USA.

[d] Radiation Laboratory, University of Notre Dame, Notre Dame, Indiana, 46556, USA.

[e] Institute of Engineering Thermophysics, Chinese Academy of Science, Beijing 100190, China

1. E. Bundgaard and F. C. Krebs, *Solar Energy Materials and Solar Cells*, 2007, 91, 954-985.

2. J. Hou, H.-Y. Chen, S. Zhang, G. Li and Y. Yang, *Journal of the American Chemical Society*, 2008, 130, 16144-16145.

3. Y. Liang, D. Feng, Y. Wu, S.-T. Tsai, G. Li, C. Ray and L. Yu, *Journal of the American Chemical Society*, 2009, 131, 7792-7799.

4. Y. Liang and L. Yu, *Accounts of chemical research*, 2010, 43, 1227-1236.

5. J. Peet, J. Kim, N. E. Coates, W. L. Ma, D. Moses, A. J. Heeger and G. C. Bazan, *Nature materials*, 2007, 6, 497-500.

6. N. Blouin, A. Michaud and M. Leclerc, *Advanced Materials*, 2007, 19, 2295-2300.

7. I. McCulloch, M. Heeney, C. Bailey, K. Genevicius, I. MacDonald, M. Shkunov, D. Sparrowe, S. Tierney, R. Wagner and W. Zhang, *Nature materials*, 2006, 5, 328-333.

8. Q. Zhou, Q. Hou, L. Zheng, X. Deng, G. Yu and Y. Cao, *Applied Physics Letters*, 2004, 84, 1653-1655.

9. Y. Liang, Z. Xu, J. Xia, S. T. Tsai, Y. Wu, G. Li, C. Ray and L. Yu, *Advanced Materials*, 2010, 22, E135-E138.

10. J. You, L. Dou, K. Yoshimura, T. Kato, K. Ohya, T. Moriarty, K. Emery, C.-C. Chen, J. Gao and G. Li, *Nature communications*, 2013, 4, 1446.

11. W. Ma, C. Yang, X. Gong, K. Lee and A. J. Heeger, *Advanced Functional Materials*, 2005, 15, 1617-1622.

12. M. T. Dang, L. Hirsch and G. Wantz, *Advanced Materials*, 2011, 23, 3597-3602.

13. W. Chen, T. Xu, F. He, W. Wang, C. Wang, J. Strzalka, Y. Liu, J. Wen, D. J. Miller and J. Chen, *Nano letters*, 2011, 11, 3707-3713.

14. J. M. Szarko, J. Guo, Y. Liang, B. Lee, B. S. Rolczynski, J. Strzalka, T. Xu, S. Loser, T. J. Marks, L. Yu and L. X. Chen, *Advanced Materials*, 2010, 22, 5468-5472.

15. L. H. Sperling, *Introduction to physical polymer science*, Wiley.com, 2005.

16. P. Reddy, S.-Y. Jang, R. A. Segalman and A. Majumdar, *Science*, 2007, 315, 1568-1571.

17. K. C. See, J. P. Feser, C. E. Chen, A. Majumdar, J. J. Urban and R. A. Segalman, *Nano letters*, 2010, 10, 4664-4667.

18. S. Wakim, B. R. Aïch, Y. Tao and M. Leclerc, *Polymer Reviews*, 2008, 48, 432-462.

19. R. d. B. Aïch, N. Blouin, A. l. Bouchard and M. Leclerc, *Chemistry of Materials*, 2009, 21, 751-757.

20. M. He, J. Ge, Z. Lin, X. Feng, X. Wang, H. Lu, Y. Yang and F. Qiu, *Energy & Environmental Science*, 2012, 5, 8351-8358.

21. T. Luo and G. Chen, *Physical Chemistry Chemical Physics*, 2013, 15, 3389-3412.

22. J. C. Duda, P. E. Hopkins, Y. Shen and M. C. Gupta, *Applied Physics Letters*, 2013, 102, 251912-251912-251915.

23. T. Tong, Y. Zhao, J. A. Hudgings and A. Majumdar, *Journal of Heat Transfer*, 2011, 133, 081601-081601.

24. Y. Jin, C. Shao, J. Kieffer, K. P. Pipe and M. Shtein, *Journal of Applied Physics*, 2012, 112, 093503-093506.

25.    O. Bubnova, Z. U. Khan, A. Malti, S. Braun, M. Fahlman, M. Berggren and X. Crispin, *Nature materials*, 2011, 10, 429-433.

26.    J. C. Duda, P. E. Hopkins, Y. Shen and M. C. Gupta, *Physical review letters*, 2013, 110, 015902.

27.    P. B. Allen and J. L. Feldman, *Physical Review B*, 1993, 48, 12581-12588.

28.    S. Shen, A. Henry, J. Tong, R. Zheng and G. Chen, *Nature Nanotechnology*, 2010, 5, 251-255.

29.    J. Liu and R. Yang, *Physical Review B*, 2010, 81, 174122.

30.    T. Zhang and T. Luo, *Journal of Applied Physics*, 2012, 112, 094304-094304-094304.

31.    T. Zhang and T. Luo, *ACS nano*, 2013.

32.    I. Osaka, M. Saito, T. Koganezawa and K. Takimiya, *Advanced Materials*, 2014, 26, 331-338.

33.    J. M. Szarko, J. Guo, Y. Liang, B. Lee, B. S. Rolczynski, J. Strzalka, T. Xu, S. Loser, T. J. Marks, L. Yu and L. X. Chen, *Advanced materials (Deerfield Beach, Fla.)*, 2010, 22, 5468-5472.

34.    A. T. Yiu, P. M. Beaujuge, O. P. Lee, C. H. Woo, M. F. Toney and J. M. Fréchet, *Journal of the American Chemical Society*, 2012, 134, 2180-2185.

35.    C. m. Cabanetos, A. El Labban, J. A. Bartelt, J. D. Douglas, W. R. Mateker, J. M. Fréchet, M. D. McGehee and P. M. Beaujuge, *Journal of the American Chemical Society*, 2013, 135, 4656-4659.

36.    D. G. Cahill, *Review of scientific instruments*, 2004, 75, 5119-5122.

37.    A. J. Schmidt, X. Chen and G. Chen, *Review of scientific instruments*, 2008, 79, 114902-114902-114909.

38.    F. P. Incropera, A. S. Lavine and D. P. DeWitt, *Fundamentals of heat and mass transfer*, John Wiley & Sons Incorporated, 2011.

39.    F. Machui, S. Rathgeber, N. Li, T. Ameri and C. J. Brabec, *Journal of Materials Chemistry*, 2012, 22, 15570-15577.

40.    A. J. Schmidt, Massachusetts Institute of Technology, 2008.

41.    B. D. Cullity and S. R. Stock, *Elements of X-ray Diffraction*, Prentice hall Upper Saddle River, NJ, 2001.

42.    W. L. Jorgensen, D. S. Maxwell and J. Tirado-Rives, *Journal of the American Chemical Society*, 1996, 118, 11225-11236.

43.    K. Do, D. M. Huang, R. Faller and A. J. Moule, *Physical Chemistry Chemical Physics*, 2010, 12, 14735-14739.

44.    T. T. To and S. Adams, *Nanoscience and Nanotechnology Letters*, 2012, 4, 703-711.

45.    D. L. Cheung, D. P. McMahon and A. Troisi, *The Journal of Physical Chemistry B*, 2009, 113, 9393-9401.

46.    N. E. Jackson, B. M. Savoie, K. L. Kohlstedt, M. Olvera de la Cruz, G. C. Schatz, L. X. Chen and M. A. Ratner, *Journal of the American Chemical Society*, 2013, 135, 10475-10483.

47.    K. J. Bowers, E. Chow, H. Xu, R. O. Dror, M. P. Eastwood, B. A. Gregersen, J. L. Klepeis, I. Kolossvary, M. A. Moraes and F. D. Sacerdoti, 2006.

48.    B. J. Leimkuhler and R. D. Skeel, *Journal of Computational Physics*, 1994, 112, 117-125.

49.    P. B. Allen, J. L. Feldman, J. Fabian and F. Wooten, *Philosophical Magazine B*, 1999, 79, 1715-1731.

50.    X. Wang, V. Ho, R. A. Segalman and D. G. Cahill, *Macromolecules*, 2013, 46, 4937-4943.

51.    T. Luo, J. Garg, J. Shiomi, K. Esfarjani and G. Chen, *EPL (Europhysics Letters)*, 2013, 101, 16001.

52.    J. C. Maxwell and J. J. Thompson, *A treatise on electricity and magnetism*, Clarendon, 1904.

53.    A. Minnich and G. Chen, *Applied Physics Letters*, 2007, 91, 073105-073105-073103.

54.    Z. Li, Y. Zhang, S.-W. Tsang, X. Du, J. Zhou, Y. Tao and J. Ding, *The Journal of Physical Chemistry C*, 2011, 115, 18002-18009.

55.    Y. Liang, Z. Xu, J. Xia, S.-T. Tsai, Y. Wu, G. Li, C. Ray and L. Yu, *Advanced Materials*, 2010, 22, E135-E138.

56.    R. Österbacka, C. An, X. Jiang and Z. Vardeny, *Science*, 2000, 287, 839-842.

57.    P. J. Brown, D. S. Thomas, A. Köhler, J. S. Wilson, J.-S. Kim, C. M. Ramsdale, H. Sirringhaus and R. H. Friend, *Physical Review B*, 2003, 67, 064203.

## Table of Contents



d polymer backbone